Available online at www.sciencedirect.com

ScienceDirect

Advances in Space Research 76 (2025) 481–496

ADVANCES IN SPACE RESEARCH (a COSPAR publication)

www.elsevier.com/locate/asr

Improving LEO short-term orbit prediction using LSTM neural network

Wei Zhang, Keke Zhang, Xingxing Li *, Jiande Huang

School of Geodesy and Geomatics, Wuhan University, 129 Luoyu Road, 430079 Wuhan, Hubei, China

Received 8 December 2024; received in revised form 20 April 2025; accepted 25 April 2025
Available online 30 April 2025

Abstract

Orbit prediction of low earth orbit (LEO) satellites is of paramount importance for LEO-augmented navigation. Currently, the most widely used approach for satellite orbit prediction in navigation domain is the dynamical propagation method, which necessitates a good understanding of orbital dynamics. However, this method is plagued by the rapid error accumulation as prediction time increases due to our limited knowledge of the complex orbit dynamics. An effective solution to this challenge is employing the machine learning algorithm, which is data-driven and requires no explicit physical knowledge, in orbit prediction of LEO satellites. We focus on improving LEO short-term (less than 120 min) orbit prediction using the long short-term memory (LSTM) neural network. To this end, we have constructed datasets of the entire year 2019 from seven LEO satellites to conduct the experiments. Historical orbit prediction errors, derived from the comparison between the dynamical-propagation-based predicted orbit and external precise orbit, along with multiple satellite status and environment features are trained to forecast future orbit prediction errors, which will subsequently serve as the compensation for improving the dynamical-propagation-based predicted orbit. Our findings reveal that the LSTM model can improve the accuracy of predicted orbit by more than 30 % for most LEO satellites with a maximum percentage around 75 %. Benefiting from the LSTM model, the prediction time for obtaining 5-cm accuracy of predicted orbit can be extended to (41.2, 42.0, 31.2, 37.9, 30.0, 86.3, 108.1) min for GRACE-C/D, Swarm-A/B/C, and Sentinel-3A/3B satellites, respectively. Additionally, generalization tests between different LEO satellites suggest that the LSTM model exhibits a commendable generalization ability when orbit prediction time is less than 30 min. As the prediction time increases, the model trained using datasets from one LEO satellite is more suitable for forecasting orbit prediction errors of multiple LEO satellites with comparable orbital altitude and orbital plane.

Keywords: Low earth orbit (LEO) satellite; Short-term orbit prediction; Long short-term memory (LSTM) neural network; Machine learning algorithm

1. Introduction

Nowadays, low earth orbit (LEO) constellation has been of great interest in the field of navigation augmentation due to the low altitude for delivering strong signals, and the fast motion for more multipath rejection and rapid change of geometric distribution which allows for shorter convergence time in precise point positioning (PPP) (Reid et al., 2016; Li et al., 2019). To fulfill the objective of LEO-augmented navigation, it is a crucial prerequisite to broadcast accurate ephemerides of LEO satellites to ground users in real time (Xie et al., 2018). Typically, the generation of these ephemerides is heavily reliant upon orbit prediction, allowing for the continuous broadcasting of up-to-date

* Corresponding author at: School of Geodesy and Geomatics, Wuhan University, 129 Luoyu Road, 430079 Wuhan, Hubei, China.
E-mail addresses: zw10147@whu.edu.cn (W. Zhang), kkzhang@whu.edu.cn (K. Zhang), xingxingli@whu.edu.cn (X. Li), jiande@whu.edu.cn (J. Huang).

https://doi.org/10.1016/j.asr.2025.04.067

LEO position and velocity information to ground users. Therefore, it is of vital importance to implement the high-accuracy orbit prediction of LEO satellites in LEO-augmented navigation domain.

Several methods have been developed presently to generate satellite predicted orbit, which mainly includes the analytical method, the polynomial fitting method, and the dynamical propagation method (Liu and Wang, 2006; He et al., 2017; Shao et al., 2020). Nevertheless, the former two methods are generally applied in areas with low-accuracy requirements such as the monitoring of space environment and the observing of space objects due to the limited prediction accuracy. The most widely used method in orbit prediction of LEO satellites is the dynamical propagation method that conducts orbit integration based on orbital dynamic information to obtain the predicted orbit (Jäggi et al., 2011). This method requires comprehensive knowledge of orbital dynamic information such as earth gravity, solar radiation pressure, and atmosphere drag. Unfortunately, our current understanding for the temporal and spatial variations of space environment is still limited, which makes it difficult to predict these variations especially for atmosphere density. As a result, the nonconservative forces are hard to be modeled accurately, resulting in the rapid accumulation of orbit prediction errors as time increases for LEO satellites (Shao et al., 2020). Previous studies have suggested that the prediction time should be confined to less than 20 min if we want to achieve orbit prediction of LEO satellites with the accuracy better than 10 cm using the dynamical propagation method (Ge et al., 2020). It means that LEO satellites need to make frequent orbit integration to fulfill the requirement of centimeter-level orbit accuracy for LEO-augmented navigation precise applications. This will undoubtedly lead to a sharp rise in system routine operation costs and difficulty, particularly for a large constellation with hundreds of LEO satellites.

In recent years, machine learning techniques have undergone significant development and are increasingly being applied in a variety of data science domains. This method learns a function or mapping from specific features to labels by identifying patterns within raw data. In other words, it is driven by data rather than explicit physical knowledge. Such an advantage provides us a great opportunity to address the issue of LEO rapidly growing prediction errors when using the dynamical propagation method.

Plenty of machine learning algorithms have been developed presently, and some of them have been successfully employed to improve the accuracy of LEO predicted orbit. Peng and Bai (2018) studied the orbit prediction of resident space objects using support vector machine (SVM). It was reported that machine learning algorithms can reduce prediction errors by more than half, with prediction durations ranging from 1 to 7 days. A comparative evaluation of three algorithms (including SVM, artificial neural network, and Gaussian processes) in terms of fitting performance and robustness was also performed (Peng and Bai, 2019). Li et al. (2020) applied the ensemble learning algorithm of boosting tree in the orbit prediction of LEO objects, and found that machine learning algorithms can improve accuracy by more than 50 % from thousands of meters to hundreds of meters for 7-day orbit prediction. Additionally, several neural network architectures, such as time-delayed neural network (TDNN) and nonlinear autoregressive with exogenous inputs (NARX) neural network, have also been confirmed to improve the accuracy of orbit prediction of LEO satellites using the simplified general perturbations 4 (SGP4) (Salleh et al., 2019; Jamil et al., 2022).

Previous literature has demonstrated that machine learning methods can effectively improve the accuracy of orbit prediction of LEO satellites. Nonetheless, most related research has focused on the accuracy improvement of daily orbit prediction for applications with low-accuracy requirements, e.g., collision avoidance. For LEO-augmented navigation, high-accuracy orbit prediction (centimeter level) within several hours or even tens of minutes arouses greater concern (Ge et al., 2020), which has rarely received attention before. Our key focus is on improving the accuracy of LEO short-term predicted orbit using machine learning algorithms and obtaining high-accuracy predicted orbit. Within this study, we classify orbit prediction within a duration of 120 min as short-term prediction. The predicted orbits of LEO satellites using the dynamical propagation method present two notable characteristics: (1). The prediction errors accumulate rapidly as time increases (temporal characteristics); (2). The accuracy of predicted orbits is influenced by the initial orbit states (long-term dependencies). Thereby, we employ the long short-term memory (LSTM) neural network (Hochreiter and Schmidhuber, 1997; Gers et al., 2000), a type of supervised machine learning algorithm, to perform the experiments. This selection is motivated by its remarkable capability of handling the problem of long-term dependencies and superior performance in time series prediction.

2. Methodology

2.1. Basic principles of the LSTM model

The LSTM model is a type of recurrent neural network (RNN) that addresses the vanishing gradient problem and the long-term dependency problem in traditional RNNs (Hochreiter and Schmidhuber, 1997; Gers et al., 2000; Yu et al., 2019). It is composed of a series of memory cells connected to each other through a set of gates that regulate the flow of information into and out of the memory cells. This allows the network to selectively retain or discard information based on its relevance to the current task.

Fig. 1 illustrates the repeating module structure in the LSTM model. The cell state $\boldsymbol{c_t}$ where is the key component of the LSTM model, responsible for selectively retaining or discarding information over long periods of time. It can be expressed as follows:

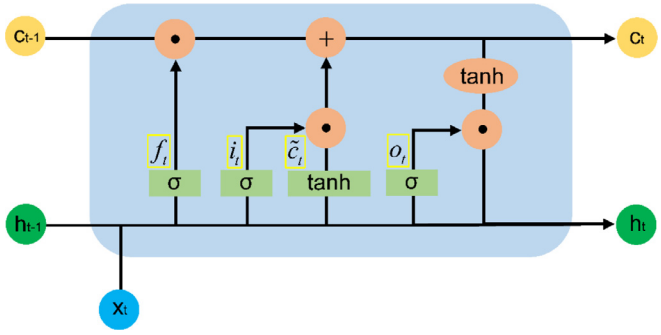

Fig. 1. Structure of repeating module in the LSTM model.

$$\boldsymbol{c_t} = \boldsymbol{f}_t \odot \boldsymbol{c}_{t-1} + \boldsymbol{i_t} \odot \widetilde{\boldsymbol{c}}_t \tag{1}$$

where $\boldsymbol{c_t} \in \mathbb{R}^{d\times 1}$, $\boldsymbol{c}_{t-1} \in \mathbb{R}^{d\times 1}$. $\boldsymbol{c}_{t-1}$ denotes the cell state of the last repeating module. d refers to the number of hidden units. $\odot$ denotes the Hadamard (element-wise) product. $\boldsymbol{i_t} \in \mathbb{R}^{d\times 1}$ and denotes the input gate. $\boldsymbol{f}_t \in \mathbb{R}^{d\times 1}$ and denotes the forget gate. $\widetilde{\boldsymbol{c}}_t \in \mathbb{R}^{d\times 1}$ and represents the candidate state which is calculated as follows:

$$\widetilde{\boldsymbol{c}}_t = \tanh(\boldsymbol{W_c x}_t + \boldsymbol{U_c h}_{t-1} + \boldsymbol{b}_c) \tag{2}$$

where $\tanh(\cdot)$ refers to the hyperbolic tangent function. $\boldsymbol{x}_t \in \mathbb{R}^{n\times 1}$ and represents the input data at a single timestep. n denotes the number of input features. $\boldsymbol{h}_{t-1} \in \mathbb{R}^{d\times 1}$ denotes the hidden state from the last repeating module. $\boldsymbol{W_c}$, $\boldsymbol{U_c}$, and $\boldsymbol{b_c}$ denote the network parameters of the model, where $\boldsymbol{W_c} \in \mathbb{R}^{d\times n}$, $\boldsymbol{U_c} \in \mathbb{R}^{d\times d}$, and $\boldsymbol{b_c} \in \mathbb{R}^{d\times 1}$.

Three gates, the input gate $\boldsymbol{i}_t$, the forget gate $\boldsymbol{f}_t$, and the output gate $\boldsymbol{o}_t$, are designed to control the delivery of information, which can be expressed as follows:

$$\begin{cases} \boldsymbol{i}_t = \sigma(\boldsymbol{W_i x}_t + \boldsymbol{U_i h}_{t-1} + \boldsymbol{b_i}) \\ \boldsymbol{f}_t = \sigma(\boldsymbol{W_f x}_t + \boldsymbol{U_f h}_{t-1} + \boldsymbol{b_f}) \\ \boldsymbol{o}_t = \sigma(\boldsymbol{W_o x}_t + \boldsymbol{U_o h}_{t-1} + \boldsymbol{b_o}) \end{cases} \tag{3}$$

where $\boldsymbol{f_t} \in \mathbb{R}^{d\times 1}, \boldsymbol{i_t} \in \mathbb{R}^{d\times 1}, \boldsymbol{o_t} \in \mathbb{R}^{d\times 1}$. $\boldsymbol{\sigma}(\cdot)$ is the Logistic function. $\boldsymbol{W} \in \mathbb{R}^{d\times n}$, $\boldsymbol{U} \in \mathbb{R}^{d\times d}$, and $\boldsymbol{b} \in \mathbb{R}^{d\times 1}$, which represent the model parameters to be learned during the training.

The hidden state $\boldsymbol{h}_t$, where $\boldsymbol{h}_t \in \mathbb{R}^{d\times 1}$ and represents the output of the current repeating module, is calculated as follows:

$$\boldsymbol{h}_t = \boldsymbol{o}_t \odot \tanh(\boldsymbol{c}_t) \tag{4}$$

The hidden state $\boldsymbol{h}_t$ and the cell state $\boldsymbol{c}_t$ can be subsequently conveyed to the next repeating module as shown in Fig. 1. After processing all repeating modules, a complete forward propagation is achieved, from which all model outputs are generated. The loss function is subsequently applied for evaluating the consistency between model outputs and real outputs. After that, the gradients of the loss function with respect to model parameters are first computed by the back-propagation through time, and then employed for updating these model parameters (Yu et al., 2019). Through multiple iterations of forward propagation and back-propagation through time, the model training is completed and we can obtain the final model parameters that are used for forecasting.

2.2. LSTM model for orbit prediction of LEO satellites

In this paper, the forecasting target of the LSTM model is orbit prediction errors of LEO satellites rather than orbits of LEO satellites. This is because our preliminary experimental results reveal that the orbit prediction accuracy is meter-level to kilometer-level if orbits of LEO satellites are directly forecasted by the LSTM model. Considering that our goal is to improve LEO short-term orbit prediction and achieve the orbit prediction with high accuracy, we employ the LSTM model to forecast orbit prediction errors of LEO satellites instead of orbits of LEO satellites as performed by Gou et al. (2023). These forecasted orbit prediction errors are further utilized to compensate for the dynamical-propagation-based predicted orbits to improve its accuracy.

We first perform the 24-h precise orbit determination (t_0 to t_1) using the reduced-dynamic method based on GNSS observations as performed by Zhang et al. (2021). After that, we can obtain the initial orbit states $\boldsymbol{z}_0$ at epoch t_0 that can be expressed as follows:

$$\boldsymbol{z}_0 = (\boldsymbol{r}_0, \dot{\boldsymbol{r}}_0, \boldsymbol{p}_0) \tag{5}$$

where $\boldsymbol{r}_0 \in \mathbb{R}^{1\times 3}$, $\dot{\boldsymbol{r}}_0 \in \mathbb{R}^{1\times 3}$, $\boldsymbol{p}_0 \in \mathbb{R}^{1\times k}$, and refer to satellite positions, velocities, and dynamics parameters at the reference epoch t_0, respectively. k denotes the number of dynamics parameters and $\boldsymbol{z}_0 \in \mathbb{R}^{1\times(6+k)}$. On the basis of the perturbating forces acting on LEO satellite, the motion equation can be constructed as follows:

$$\ddot{\boldsymbol{r}}(t) = -\frac{GM}{|\boldsymbol{r}|^3}\boldsymbol{r} + f(\boldsymbol{r}, \dot{\boldsymbol{r}}, \boldsymbol{p}, t) \tag{6}$$

in which $\boldsymbol{r}$, $\dot{\boldsymbol{r}}$, $\ddot{\boldsymbol{r}}(t)$, and $\boldsymbol{p}$ denotes satellite positions, velocities, accelerations, and dynamics parameters at epoch t, respectively. G is the gravity constant and M is the mass of the Earth. f represents the sum of all perturbing forces beyond the centered term of the Earth's gravity. Combining (5) and (6), we can obtain the differential equation as follows:

$$\begin{cases} \dot{\boldsymbol{z}}(t) = g(z(t), t) \\ z(t_0) = \boldsymbol{z}_0 \end{cases} \tag{7}$$

where $\dot{\boldsymbol{z}}(t)$ refers to the derivative of the orbit states $\boldsymbol{z}(t)$ at epoch t with respect to the time. g is the function of $\dot{\boldsymbol{z}}(t)$ with respect to $\boldsymbol{z}(t)$ and t. In light of the complexity of the perturbing forces acting on LEO satellite, we cannot directly obtain the analytical solution of (7). But with the numerical integration method, the orbit states $\boldsymbol{z}(t)$ at epoch t can still be determined. We further extend the 24-h integration time (t_0 to t_1) to 26 h (t_0 to t_2), indicating that the

former 24-h orbit arc (t_0 to t_1) represents the observed arc and the latter orbit 2-h arc (t_1 to t_2) represents the predicted arc.

During the numerical integration, LEO positions are first obtained, and then utilized to compute orbit errors as follows:

$$\boldsymbol{y} = \boldsymbol{r} - \widetilde{\boldsymbol{r}} \tag{8}$$

where $\boldsymbol{r}$ denotes LEO positions from the orbit integration and $\widetilde{\boldsymbol{r}}$ refers to LEO positions from external precise science orbit (PSO) products. $\boldsymbol{y}$ denotes orbit errors in the observed arc and orbit prediction errors in the predicted arc. Apart from orbit errors of LEO satellites, multiple features of satellite status and space environment ($\boldsymbol{x}$), such as satellite positions and atmosphere density, can be obtained from the orbit integration. The datasets for LSTM model training and forecasting are constructed by $\boldsymbol{x}$ and $\boldsymbol{y}$. Fig. 2 illustrates the input and output data generation for LSTM model training and forecasting. Our datasets are constructed by multiple orbit arcs, each of which consists of one 24-h observed arc and one 2-h predicted arc. The basic input window for model training/forecasting is represented by a $m \times (n+1)$ matrix, in which m denotes the length of the input window and n denotes the number of selected features. It indicates that the model input involves orbit errors and multiple features with a specific length m. The outputs of the LSTM model are orbit prediction errors ($y_i, i > 0$, yellow part in the figure). One $m \times (n+1)$ input window corresponds to one output (orbit prediction error of the adjacent epoch).

In the course of the model training, orbit prediction errors ($y_i, i > 0$) are known and computed by the comparing the predicted orbits and external PSO products. For one orbit arc, the first $m \times (n+1)$ input window is constructed which is sorely based on the 24-h observed arc ("window 1" in Fig. 2). The first output is y_1, representing the orbit prediction error of the first epoch. "window 1" and y_1 compose the first input–output pair. Then "window 1" shifts by one step to "window 2" and y_1 shifts to y_2 for generating the second input–output pair as performed by Şimşek et al. (2025). The shifting operation will be carried out continuously on this arc until the last output y_p in which the subscript p refers to the length of the anticipated predicted orbit. For instance, p equals to 240 provided that the experimental prediction time is 120 min with the interval of 30 s. Then the similar operation will be performed on all orbit arcs in the training datasets, from which we can obtain all inputs and outputs for the model training.

For the model forecasting, the model inputs are generated using the method as performed in the model training. The primary difference is that orbit prediction errors ($y_i, i > 0$) are unknown and need to be forecasted. Based on "window 1" and the trained model, we can obtain the first forecasted orbit prediction error ($\widehat{y}_1$). Afterwards, $\widehat{y}_1$ replaces y_1 in "window 2" which is subsequently utilized to forecast the second orbit prediction error ($\widehat{y}_2$). For the subsequent input windows, y_i is substituted by $\widehat{y}_i$ for forecasting the orbit prediction errors, ensuring that each forecasting is based on the known data (green part in the figure) and previous forecasted orbit prediction errors (yellow part in the figure). These forecasted orbit prediction errors will be further employed to compensate for the original predicted orbits to generate the compensated predicted orbits as follows:

$$\widehat{\boldsymbol{r}} = \boldsymbol{r} - \widehat{\boldsymbol{y}} \tag{9}$$

where $\widehat{\boldsymbol{r}}$ represents the final predicted orbits improved by the LSTM model.

2.3. Evaluation metrics

In this study, we adopt the metric P to evaluate the forecasting performance of the LSTM model following Peng and Bai (2018). This metric is defined as the ratio of the

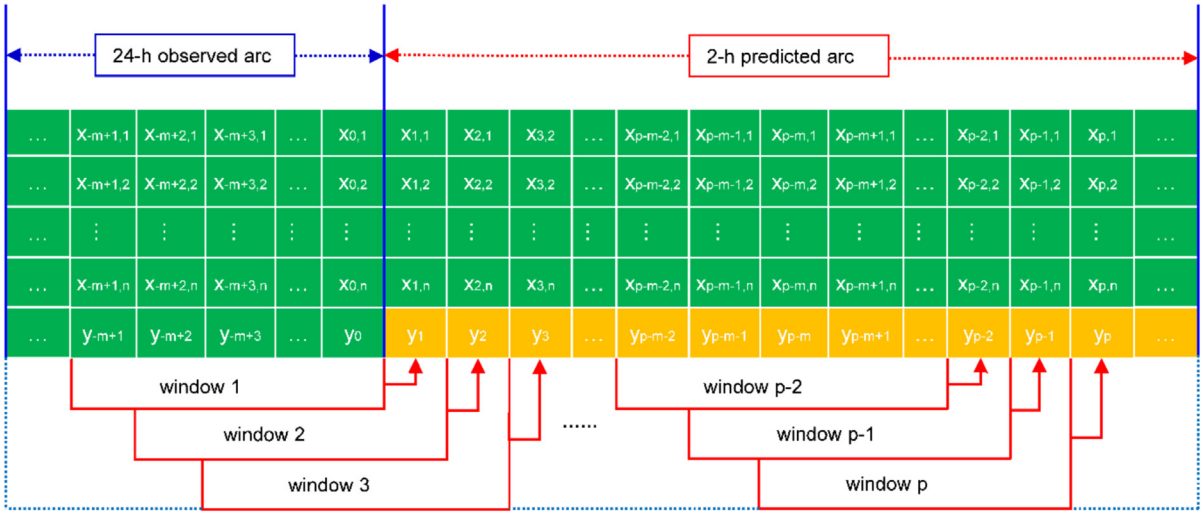

Fig. 2. Input and output data generation of LSTM training and forecasting (Green parts represent the data obtained before the forecasting; Yellow parts represent the data to be forecasted; Each row refers to the time series of one feature and each column refers to the feature set in one epoch).

cumulative absolute deviations between the true orbit prediction errors ($\boldsymbol{y}$) and the LSTM-forecasted results ($\widehat{\boldsymbol{y}}$), to the cumulative absolute values of $\boldsymbol{y}$ in the testing dataset, which can be expressed as follows:

$$P = \frac{\sum_{i=1}^{s} |y_i - \widehat{y}_i|}{\sum_{i=1}^{s} |y_i|} \tag{10}$$

where s denotes the number of testing samples. It should be noted that $\widehat{y}_i$ herein represents the direct forecasted results of orbit prediction errors from the LSTM model (used to compensate for the original predicted orbits as indicated in (9)), but not the final errors of LSTM-compensated predicted orbits. The metric P quantifies the consistency between the true results and LSTM-forecasted results, with a lower boundary of zero (indicating perfect agreement) and no upper boundary. Smaller values of P reflect better agreement between the true results and LSTM-forecasted results, thus better performance of the trained LSTM model (Peng and Bai, 2018).

As mentioned previously, our goal is to improve LEO short-term orbit prediction using the LSTM model and achieve orbit prediction with high accuracy. Accordingly, in addition to the metric P, the accuracy of predicted orbits compensated by the LSTM model is also assessed. Forecasted results of orbit prediction errors from the LSTM model are used to compensate for the original predicted orbits for generating the compensated predicted orbits ($\widehat{\boldsymbol{r}}$) as indicated in (9), which are further compared with external PSO products ($\widetilde{\boldsymbol{r}}$) to compute the differences as follows:

$$\boldsymbol{e} = \widehat{\boldsymbol{r}} - \widetilde{\boldsymbol{r}} \tag{11}$$

where $\boldsymbol{e}$ represents the final errors of predicted orbits compensated by the LSTM model, serving as the indicator of the accuracy of LSTM-compensated predicted orbits.

3. Data collection and preprocessing

Fig. 3 illustrates the data processing framework. First, initial orbit states generated from precise orbit determination will be used to perform orbit integration to obtain the 24-h observed orbit and the 2-h predicted orbit and multiple features. Orbit comparison between observed/predicted orbit and external PSO products is subsequently conducted to compute orbit (prediction) errors. Orbit (prediction) errors and features are then divided into training data for the training of the LSTM model and testing data for the validation of model generalization ability. Finally, we can obtain the forecasted orbit prediction errors from the forecasting process which will be assessed by metric P. In addition, these forecasted orbit prediction errors are further utilized to compensate for dynamic predicted orbit. Subsequently, the improved orbit accuracy can be evaluated by comparing the compensated predicted orbit and external PSO products.

3.1. Construction of datasets

Seven LEO satellites with different altitudes and inclinations, including GRACE-C/D, Swarm-A/B/C, and Sentinel-3A/3B have been selected as shown in Table 1. PSO products of GRACE-C/D and Swarm-A/B/C are respectively computed by the Jet Propulsion Laboratory (JPL) and European Space Agency (ESA), while the Copernicus Precise Orbit Determination service (CPOD) is responsible for the generation of Sentinel-3A/3B PSO products (Olsen et al., 2013; Calero et al., 2019; Wen et al., 2019). Precise orbit determination is performed using the onboard GNSS data from these LEO satellites from day of year (DOY) 001 in 2019 to DOY 365 in 2019 to

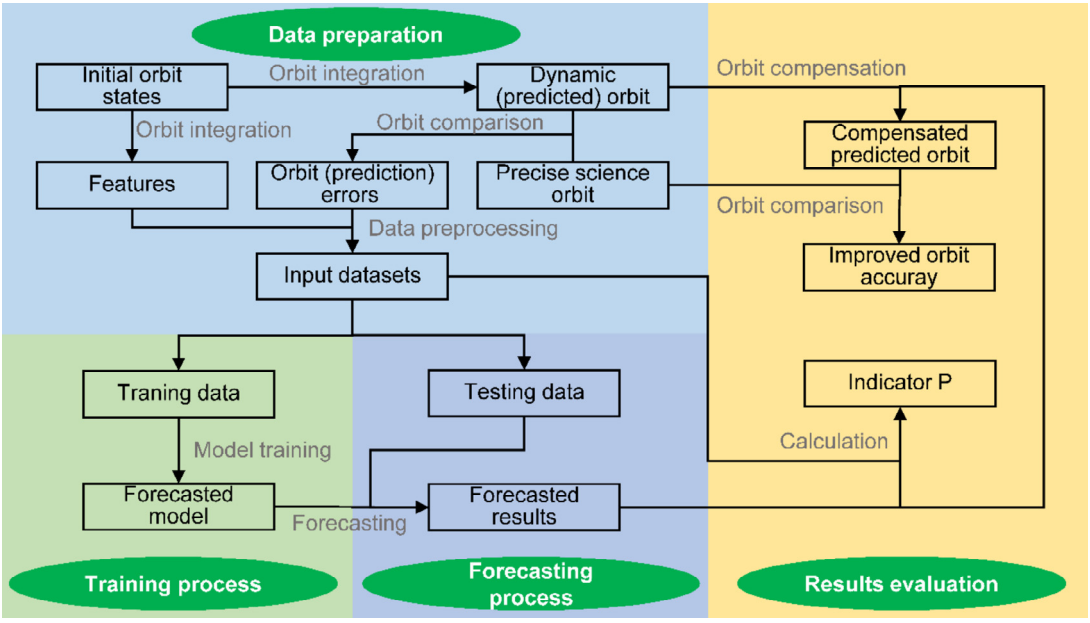

Fig. 3. Data processing framework in LEO short-term orbit prediction using the LSTM model.

Table 1
Information of seven selected LEO satellites for orbit prediction.

Mission	Satellite/Abbreviation	Altitude/km	Inclination/°	PSO source
GRACE-FO	GRACE-C/GRAC	490	89	JPL
	GRACE-D/GRAD	490	89	
Swarm	Swarm-A/SWAA	460	87.35	ESA
	Swarm-B/SWAB	530	87.75	
	Swarm-C/SWAC	460	87.35	
Sentinel-3	Sentinel-3A/SE3A	814.5	98.65	CPOD
	Sentinel-3B/SE3B	814.5	98.65	

obtain the initial orbit states of each day (Zhang et al., 2021). After that, the orbit integration is conducted based on these initial orbit states to acquire 2-h predicted orbit as well as the feature sets as depicted in Fig. 2. A total of 365 predicted orbit arcs with the length of 120 min will be used in the subsequent experiments.

During the orbit integration, all variables with a total number of 34 that might be associated with the orbit prediction errors are output to serve as the feature collection for training and forecasting. As shown in Table 2, these features consist of six orbital elements of the LEO satellite (E_A, E_I, E_O, E_W, E_M, E_E), positions of the Sun (PA_Su, PC_Su, PR_Su), density of the atmosphere (DEN), geomagnetic ap index (GEO_A), F10.7 index of the solar radio flux (SOL_F), current epoch (Epo), total accelerations (AA, AC, AR), and accelerations of the Earth gravity (AA_Gr, AC_Gr, AR_Gr), N-body (AA_PM, AC_PM, AR_PM), relativity (AA_Re, AC_Re, AR_Re), atmosphere drag (AA_At, AC_At, AR_At), empirical accelerations (AA_Emp, AC_Emp), solar radiation pressure (AA_SR, AC_SR, AR_SR). It should be pointed out that the reference frame of all positions and accelerations in the feature collection, as well as the orbit prediction errors, has been uniformly converted to the satellite orbit reference frame that comprises three axes, namely along-track (A), cross-track (C), and radial (R).

3.2. Processing strategies

The dynamic models employed in the orbit integration have been listed in Table 2. Conservative forces including the Earth gravity, N-body perturbation, and relativity are described using the high-fidelity models. For non-conservative forces, several models have been employed to describe solar radiation pressure and atmosphere drag. However, these models cannot accurately represent non-conservative forces due to their strong correlation with the space environment and spacecraft characteristics for LEO satellites. Following the concept of reduced-dynamic orbit determination, the one-cycle-per-revolution empirical accelerations in the along-track and the cross-track directions are applied to absorb unmodeled force errors.

Table 3 displays the configuration of the LSTM model. Datasets have been divided into two parts, wherein 80 % of the data are used for training the model and the remaining 20 % are used for testing the performance and generalization ability of the model. The training epoch is set to 6, and the batch size is set to 32. Note that the training epoch mentioned here specifically refers to one complete cycle of training process, distinguishing it from the aforementioned epoch. The basic structure of the LSTM model consists of five neural network layers, including three LSTM layers,

Table 2
Feature sets and the corresponding dynamic models.

Features	Abbreviation	Dynamic model
Accelerations of Earth gravity	AA_Gr, AC_Gr, AR_Gr	EIGEN6S4: order and degree 120
Accelerations of N-body	AA_PM, AC_PM, AR_PM	DE421
Accelerations of relativity	AA_Re, AC_Re, AR_Re	IERS2010 (Petit and Luzum, 2010)
Empirical accelerations	AA_Emp, AC_Emp	One-cycle-per-revolution acceleration (sine and cosine terms in the along-track and cross-track directions)
Accelerations of solar radiation pressure	AA_SR, AC_SR, AR_SR	Box-wing macro-model (Fernández Martìn 2016; Montenbruck et al., 2018; Wen et al., 2019)
Accelerations of atmosphere drag	AA_At, AC_At, AR_At	NRLMSISE00 thermosphere model (Picone et al., 2002)
Density of atmosphere	DEN	
Total accelerations	AA, AC, AR	–
Six orbital elements of LEO satellite	E_A, E_I, E_O, E_W, E_M, E_E	–
Positions of the Sun	PA_Su, PC_Su, PR_Su	–
Geomagnetic ap index	GEO_A	–
F10.7 index of the solar radio flux	SOL_F	–
Current epoch	Epo	–

Table 3
Detailed information of the LSTM model configuration.

Item	Value
Training/Testing data distributions	80 % for training and 20 % for testing
Number of training epoch	6
Batch size	32
Neuron number	10
Layer number	5
Dropout rate	0.2
Loss function	Mean Squared Error (MSE)
Optimizer	Root Mean Square Propagation (RMSProp)
Activation function	Rectified Linear Unit (ReLU) (Nair and Hinton, 2010)

one Dropout layer with a dropout rate of 0.2, and one Dense layer. Mean Squared Error (MSE) is selected as the loss function. Additionally, we choose Root Mean square Propagation (RMSProp) as the optimizer and Rectified Linear Unit (ReLU) as the activation function.

3.3. Feature selection

It is generally recognized that excessive features in machine learning model training can lead to overfitting problems and increase the computational complexity and training time of the model (Pintas et al., 2021). Our datasets include 34 features, which may be overabundant for the LSTM model, thus leading to the performance degradation. It is, consequently, indispensable to conduct feature selection to discard redundant features and obtain the most informative ones.

We first evaluate the contribution of each feature to orbit prediction errors using the extreme gradient boosting (XGBoost) model which is a scalable machine learning system of tree boosting proposed by Chen and Guestrin (2016). Fig. 4 illustrates the importance scores of all features related with orbit prediction errors of GRACE-C satellite in three directions. Note that the feature scores have been normalized to a scale from 0 to 1. It can be observed from the figure that the "Epo" feature contributes the most to the orbit prediction errors for all three directions, which can be easily understood by the fact that orbit prediction errors accumulate with time. The importance ranking of the remaining features in all directions presents a roughly similar distribution. Based on this, we will apply the same feature collection in the LSTM model for predicted orbit errors in different directions.

Considering that our experiments involve multiple LEO satellites, we also compare the feature importance ranking for different LEO satellites. Fig. 5 displays the feature importance scores with respect to orbit prediction errors in the along-track direction for three LEO satellites from different missions. Despite that the "Epo" feature contribute the most to orbit prediction errors, the importance ranking of the remaining features presents larger disparity between different LEO satellites, especially for Sentinel-3A satellite. This can be explained by the orbital altitude difference among these LEO satellites. Different from the other two satellites, Sentinel-3A satellite orbits at an altitude exceeding 800 km, making the features associated with the Sun such as "PC_Su" more dominant. We also observe that "SOL_F" plays a more significant role for orbit prediction errors of Sentinel-3A satellite than those of GRACE-C and Swarm-A satellites. Although "SOL_F" is only applied for computing atmosphere density, which exerts a greater influence on GRACE-C and Swarm-A satellites due to their lower orbital altitude, Sentinel-3A satellite exhibits a higher area-mass ratio. Consequently, the orbit prediction errors of Sentinel-3A satellite are likely more sensitive to variations in solar flux than those of Swarm-A and GRACE-C satellites. According to these results, we will apply a specific feature collection in the training and forecasting for individual LEO satellites according to the corresponding feature sensitivity.

Following the feature importance ranking is feature filtering according to feature correlations because some features are strongly correlated such as atmosphere density and accelerations of atmosphere drag. Herein, the Spearman's rank correlation method is adopted to evaluate correlations between different features. Fig. 6 displays the feature correlations of GRACE-C satellite. It should be pointed out that the former 20 features are selected in accordance with the feature ranking results. The correlation threshold is set to an empirical value of 0.5. The left subgraph shows the original correlations between these 20 features. As expected, some features present strong correlations such as Sun position (PA_Su) and accelerations of solar radiation pressure (AA_SR). During feature filtering, one feature in individual strongly correlated feature pairs will be discarded. Fifteen features are left finally, which will be applied in subsequent experiments.

4. Experimental results

In this section, we will perform the orbit prediction using the LSTM model for different LEO satellites. The prediction time is set from 10 min to 120 min with an interval of 10 min. The impact of model configuration including the number of features (NF) and length of sliding window (WL) on model performance is investigated first. The optimal configuration will be subsequently applied in the LSTM model for different LEO satellites, which will be evaluated by the metric P and the improved orbit prediction accuracy. Additionally, generalization tests between different LEO satellites are carried out to validate the generalization ability of the LSTM model.

4.1. Optimization of the LSTM model configuration

Basic configuration of the LSTM model has been given in Table 3. In addition to these parameters, two key factors, NF and WL, as depicted in Fig. 2, will directly

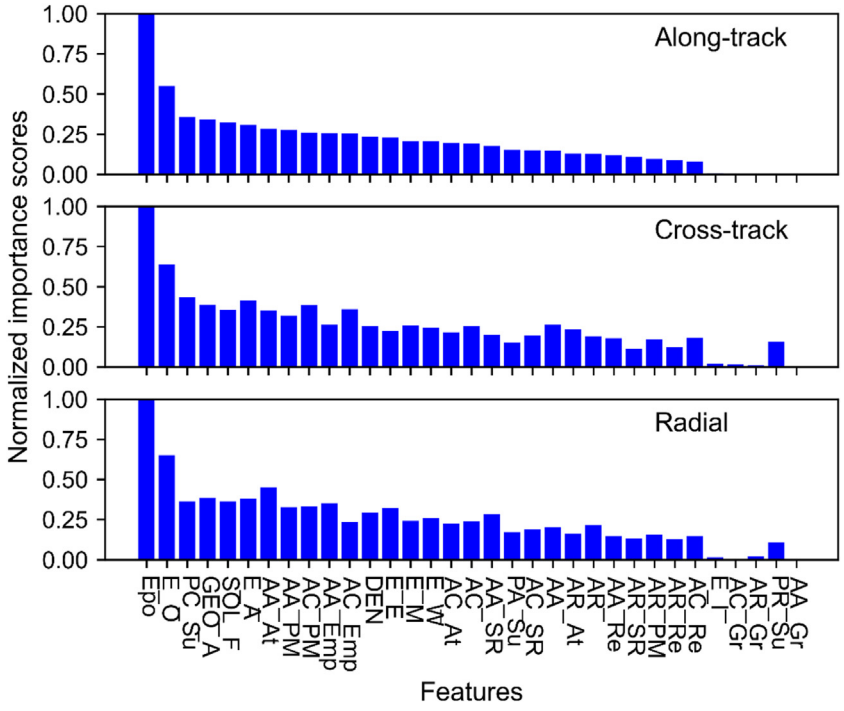

Fig. 4. Normalized feature importance scores with respect to orbit prediction errors of GRACE-C satellite in three directions.

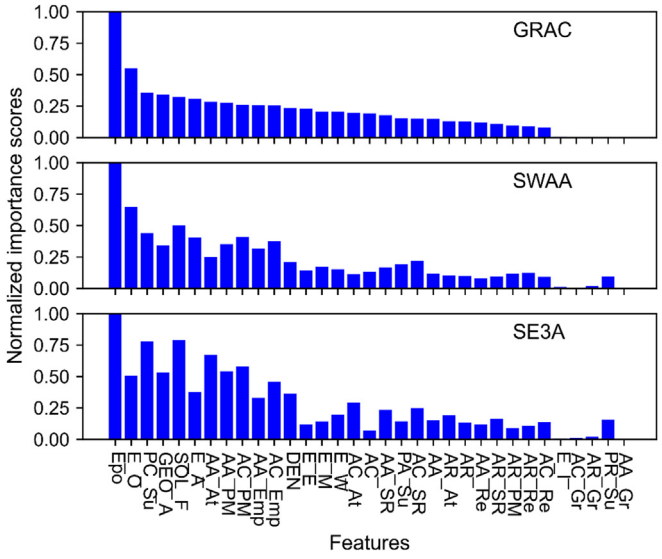

Fig. 5. Normalized feature importance scores with respect to orbit prediction errors in the along-track direction for three LEO satellites.

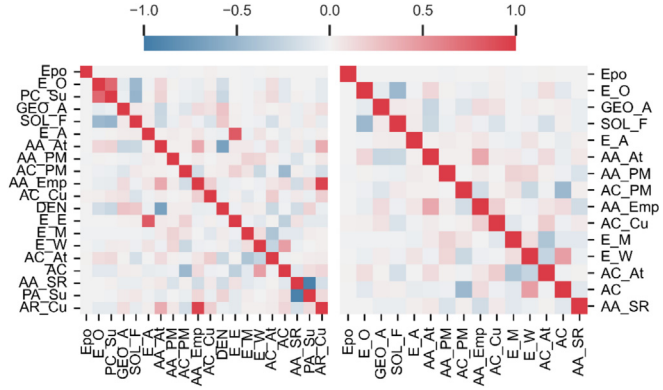

Fig. 6. Feature correlations of GRACE-C satellite (Left: the former 20 features according to feature importance scores; Right: the filtered features with correlations less than 0.5).

influence the performance of the LSTM model. To investigate the impact of these two factors on model performance, numerous solutions with different NFs and WLs have been designed. NF is set from one to sixteen with an interval of one. Note that the 1-NF solution only contains historical orbit prediction errors. Then we add one feature to the former solution each time as a new NF solution according to the importance ranking of filtered features. For adapting WL to the length of individual prediction time, we set different WLs for individual prediction time as follows:

$$WL_t = \frac{k}{20} \cdot t, \mathrm{k} = 1, 2, 3 \ldots 20 \tag{12}$$

in which t refers to prediction time (Unit: epoch) and WL_t denotes the epoch number of corresponding WL. k refers to the proportional coefficient with the range from one to twenty. It is indicated from this equation that WL varies from one-twentieth to the same length of the corresponding prediction time, allowing for a comprehensive assessment of the impact of WL on model performance. Consequently, we obtain 320 solutions for each prediction time. We first compute the P values of these 320 solutions, and then normalize them to the range from 0 to 1 using the min–max normalization as follows:

$$\widetilde{P}^{t}_{WL,NF} = \frac{P^{t}_{WL,NF} - P^{t}_{min}}{P^{t}_{max} - P^{t}_{min}} \tag{13}$$

where $P^{t}_{WL,NF}$ denotes the P value of the solution with a specific WL and NF under the prediction time t and $\widetilde{P}^{t}_{WL,NF}$ denotes the normalized P value. P^{t}_{min} and P^{t}_{max} refer to the minimum and maximum P value of all 320 solutions under the prediction time t, respectively.

Fig. 7 displays the maps of normalized P values of all 320 solutions for each prediction time using the LSTM model for GRACE-C satellite. For the 10 min-prediction, the left upper part of the map presents a large magnitude, indicating poor performance of the LSTM model with a small WL. By comparison, an increase in WL can contribute to the reduction of P values. We also notice that the model with a large NF still presents poor performance even with a large WL. This can be explained by the fact that too many features might lead to overfitting problems, especially for the extremely short prediction arc.

As the prediction time increases, a pronounced variation of the map distribution can be noticed. On the one hand, the large P values from the left upper part of the map decrease gradually and reach a similar magnitude as the remaining part of the map when the prediction time exceeds 20 min. This suggests that the improvement of model performance brought by the enlargement of WL gets reduced as the prediction time increases, and a large WL is well suited only for the prediction time less than 20 min. On the other hand, we can observe that P values from the lower part of the map gain enlargement and exhibit a large magnitude, especially when the prediction time exceeds 60 min. This implies that a small NF will lead to the degradation of model performance, and a larger NF is more suitable for the orbit prediction of LEO satellites greater than 60 min. The optimal configuration of LSTM model concerning NF and WL for GRACE-C satellite is provided in Table 4.

4.2. Forecasted results of different LEO satellites

Based on the experimental results from the previous section, the optimal configuration concerning NF and WL is

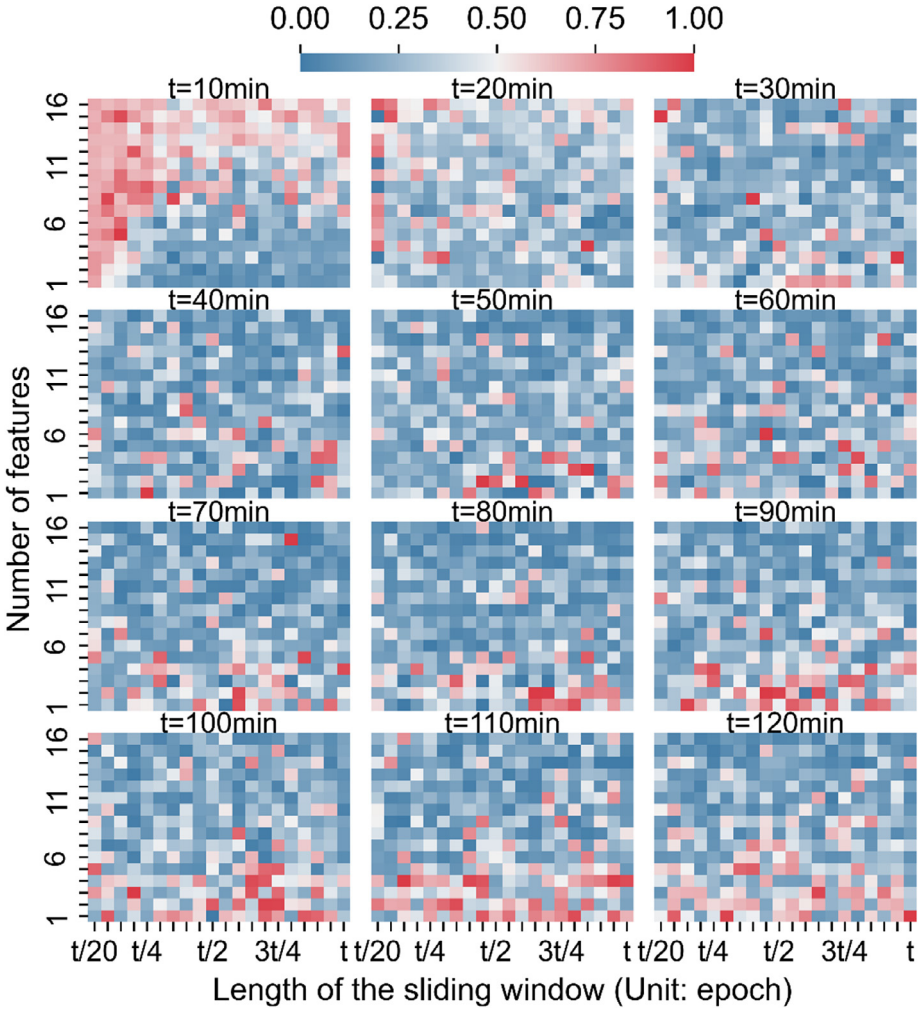

Fig. 7. Normalized P results of GRACE-C satellite with different NFs and WLs for different prediction time (The squares with different colors denote the normalized P values with a range from 0 to 1; "t" refers to the corresponding prediction time with the unit of epoch).

Table 4
Optimal configuration of LSTM model for GRACE-C satellite.

Prediction time/min	Optimal NF	Optimal WL	
		Relative value (k)	Absolute value/epoch
10	3	7	7
20	3	1	2
30	4	9	27
40	4	9	36
50	4	7	35
60	4	13	78
70	9	20	140
80	6	9	72
90	16	7	63
100	13	4	40
110	14	14	154
120	14	16	192

employed for training and forecasting in this section. Orbit prediction errors of one typical testing orbit arc with 120 min duration in three directions for GRACE-C satellite are illustrated in Fig. 8. Orbit prediction errors in the along-track direction present the most pronounced growth as the prediction time increases which can reach a maximum magnitude of −120 cm. By comparison, orbit prediction errors in the cross-track and radial directions accumulates slowly, varying in the range of [-5, 10] and [0, 20] cm, respectively. It suggests that the key to improving LEO short-term orbit prediction lies in reducing the growing of orbit prediction errors in the along-track direction. Our forecasted results using the LSTM model agree well with the results from the dynamical propagation in three directions, indicating the good performance of the LSTM model in LEO short-term orbit prediction preliminarily.

To evaluate the performance of the LSTM model quantitatively, we calculate the root mean square (RMS) value of orbit differences between PSO products and predicted orbits with and without compensation of the LSTM model for each orbit arc of GRACE-C satellite. These RMS values from individual prediction time are subsequently used to compute the mean value as displayed in Fig. 9. With the compensation of the forecasted results, orbit differences get reduced markedly for individual prediction time. The maximum reduction is achieved by the 10 min-prediction which can reach (59.3 %, 74.8 %, 71.1 %) in three directions, respectively. As the prediction time increases, the P value gains enlargement gradually but is still less than 0.8. When the prediction time increases to 120 min, the mean RMS of the results from the dynamical propagation is (25.4, 2.5, 4.4) cm in three directions, which decreases to (13.0, 1.6, 3.1) cm after the compensation from the LSTM model. The corresponding mean RMS reduction of orbit errors reach (49.4 %, 34.3 %, 29.9 %) and the P value is (0.49, 0.63, 0.64). Overall, the improvement of predicted orbit accuracy brought by the LSTM model exceeds 30 % with a maximum value around 75 % and the P value is less than 0.8 with a minimum value around 0.2.

Given that the Signal-in-Space Ranging Error (SISRE) is more significant for ground users in LEO-augmented navigation, we further compute the SISRE results that only consider orbit errors and no clock errors for each LEO satellite as indicated by Reid et al. (2016). Fig. 10 depicts these SISRE results of predicted orbits with and without compensation of the LSTM model of seven LEO satellites. We can notice that orbit differences of Sentinel-3A/3B present the smallest magnitude among these satellites. This can be explained by the high orbital altitude (more than 800 km) of Sentinel-3A/3B which makes the satellite less

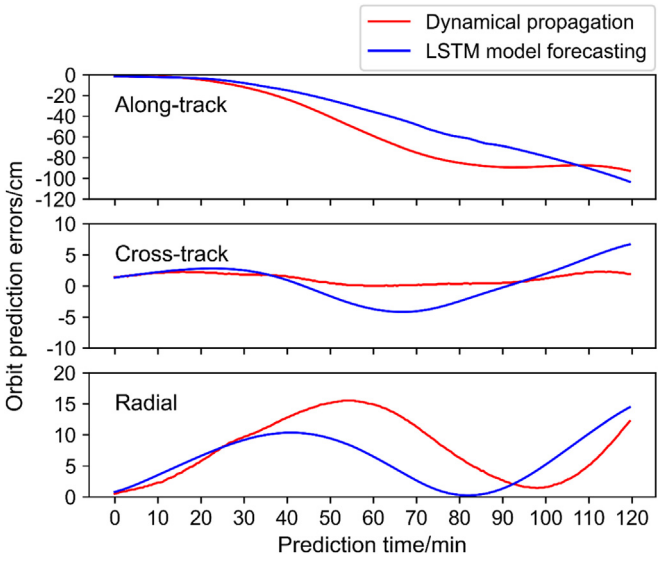

Fig. 8. Orbit prediction errors from the dynamical propagation and the LSTM model forecasting in three directions from one typical testing orbit arc for GRACE-C satellite (Red lines represent the dynamical propagation and blue lines represent the LSTM model forecasting).

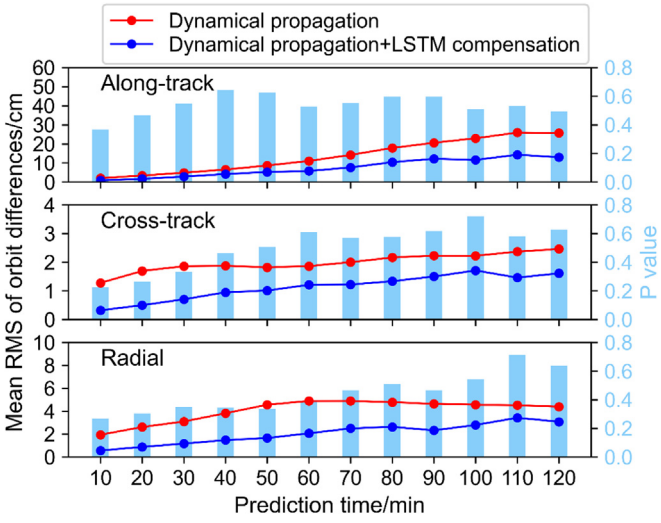

Fig. 9. Mean RMS of orbit differences between PSO products and predicted orbits with and without compensation of the LSTM model in three directions of GRACE-C satellite (Red lines represent results without compensation; Blue lines represent results with compensation; Light blue bars represent the results of P).

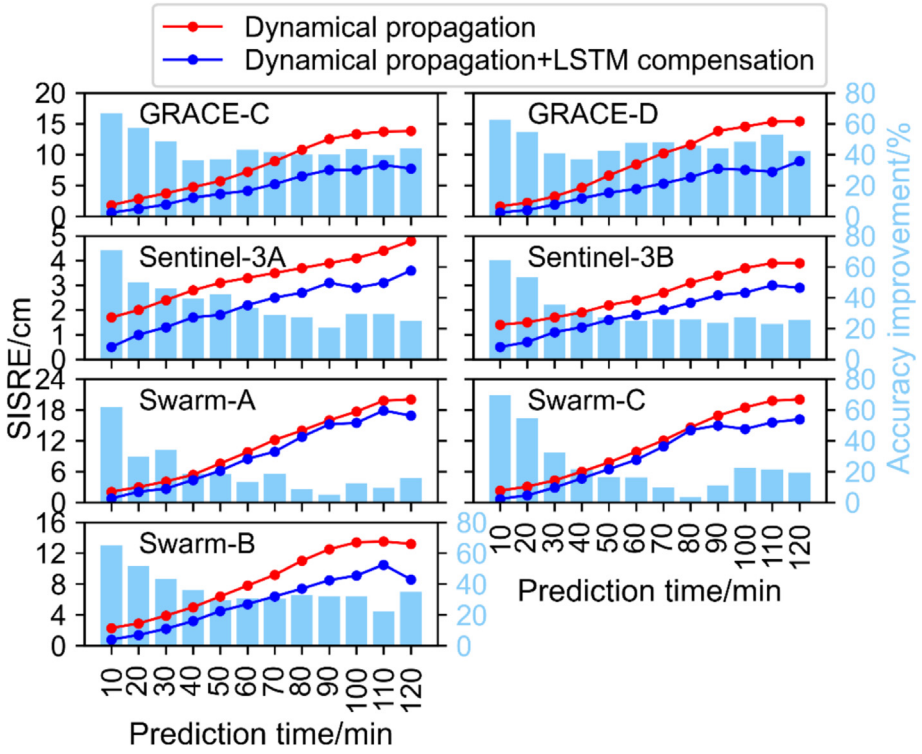

Fig. 10. SISRE of predicted orbits with and without compensation of the LSTM model of seven LEO satellites (Red lines represent results without compensation; Blue lines represent results with compensation; Light blue bars represent the accuracy improvement brought by LSTM model).

affected by atmosphere drag, leading to a slower growing of orbit prediction errors. The results of the satellites from the same mission present a similar magnitude except for Swarm satellites. In comparison with the results of Swarm-B, the SISRE of Swarm-A/C is much larger because the orbital altitude of Swarm-B (530 km) is higher than that of Swarm-A/C (460 km).

A noticeable SISRE reduction brought by the LSTM compensation can be observed for all LEO satellites. For the prediction time of 10 min, 60 min, and 90 min, the reduction of SISRE can reach (66.6 %, 43.2 %, 39.3 %) for GRACE-C satellite, (65.2 %, 30.0 %, 32.3 %) for Swarm-B satellite, and (68.3 %, 34.9 %, 20.2 %) for Sentinel-3A satellite. When the prediction time increases to 120 min, the accuracy of predicted orbit improved by the LSTM model is (12.4, 14.3, 27.0, 14.0, 25.9, 6.1, 4.9) cm with an improvement of (44.2 %, 41.9 %, 15.6 %, 34.0 %, 19.0 %, 26.1 %, 26.3 %) for GRACE-C/D, Swarm-A/B/C, and Sentinel-3A/3B satellites, respectively. These results are encouraging and suggest that our LSTM model can significantly improve the accuracy of LEO short-term prediction for different LEO satellites with different orbital altitudes.

Currently, the accuracy of ultra-rapid orbit products based on orbit prediction for global positioning system (GPS) satellites is approximately 5 cm, allowing for real-time precise point positioning (Kazmierski et al., 2018; Lou et al., 2022). Following this accuracy standard, we employ a 5 cm orbit prediction accuracy to evaluate the model performance. Table 5 presents the maximum prediction time for maintaining the orbit prediction accuracy (SISRE) better than 5 cm for all LEO satellites. It can be noticed that the compensation from the LSTM model can contribute to an evident extension of the prediction time for achieving 5-cm orbit prediction accuracy. With the improvement of the LSTM model, the 5-cm orbit prediction accuracy can be achieved for the prediction time of (68.2, 66.7, 43.3, 55.6, 41.7, 172.9, 181.4) min for GRACE-C/D, Swarm-A/B/C, and Sentinel-3A/3B satellites, respectively. As reported by Ge et al. (2020), the 60-min orbit prediction accuracy was roughly 5 cm when using accelerometer data with the calibration parameters of biases and scale factors in each axis for GRACE-A satel-

Table 5
Maximum prediction time for maintaining the orbit prediction accuracy (SISRE) better than 5 cm for all LEO satellites (Unit: minute).

Satellite	Orbit prediction accuracy of 5 cm	
	Dynamical propagation	Dynamical propagation + LSTM compensation
GRACE-C	43.0	68.2
GRACE-D	42.0	66.7
Swarm-A	36.9	43.3
Swarm-B	40.0	55.6
Swarm-C	34.1	41.7
Sentinel-3A	129.4	172.9
Sentinel-3B	140.1	181.4

lite. Considering the similarity of LEO mission and orbital altitude of GRACE-A and GRACE-C satellites, we compare the results of these two satellites, and reveal that our orbit prediction results of GRACE-C satellite present higher accuracy (4.1 cm for the 60-min orbit prediction). This demonstrates the pronounced advantage of our method (dynamical propagation + LSTM compensation) for short-term orbit prediction of LEO satellites. These findings suggest that the prediction time for obtaining predicted orbit with 5-cm accuracy can be extended to more than 30 min for all LEO satellites after the compensation from the LSTM model. Consequently, the frequency for conducting orbit integration can be significantly lowered, contributing to the reduction of system routine operation costs and difficulty in LEO-augmented navigation applications.

4.3. Generalization tests between different LEO satellites

The current LEO constellation under construction usually consists of hundreds of, even thousands of LEO satellites (Reid et al., 2016; Del Portillo et al., 2019). To improve the accuracy of orbit prediction of LEO satellites for such large constellations, a significant amount of computing resources and time will be required if the model training is performed for individual LEO satellites. In order to improve the training efficiency and save the computing resources, one effective way is to apply the model trained by datasets from one LEO satellite to forecast orbit prediction errors of multiple LEO satellites. It is, therefore, of vital significance to validate the generalization ability of the LSTM model between different LEO satellites.

In this section, six solutions concerning three LEO missions have been designed to validate the generalization ability of the LSTM model. Datasets of one LEO satellite selected from individual missions are used for training. The trained model of this satellite is subsequently employed to forecast orbit prediction errors of the satellite from the same mission as well as the satellite from another mission. Fig. 11 illustrates the SISRE results of predicted orbits with and without compensation of the LSTM model from the generalization tests between different LEO satellites. It should be noted that the solution "LEO1_LEO2" represents applying the trained model of LEO1 to forecast the orbit prediction errors of LEO2. For the 10 min-prediction, the LSTM model presents superior performance in improving the orbit prediction accuracy by more than 60 % for all solutions. When the prediction time increases to 30 min, the improvement can still reach more than 20 % for all solutions. This indicates that the LSTM model is of good generalization ability in tests between different LEO satellites when the prediction time is less than 30 min.

As the prediction time increases further, an evident improvement of the orbit accuracy brought by the LSTM model is still visible for "GRAC_GRAD" solution which can reach 54.5 % for the 120 min-prediction. In contrast,

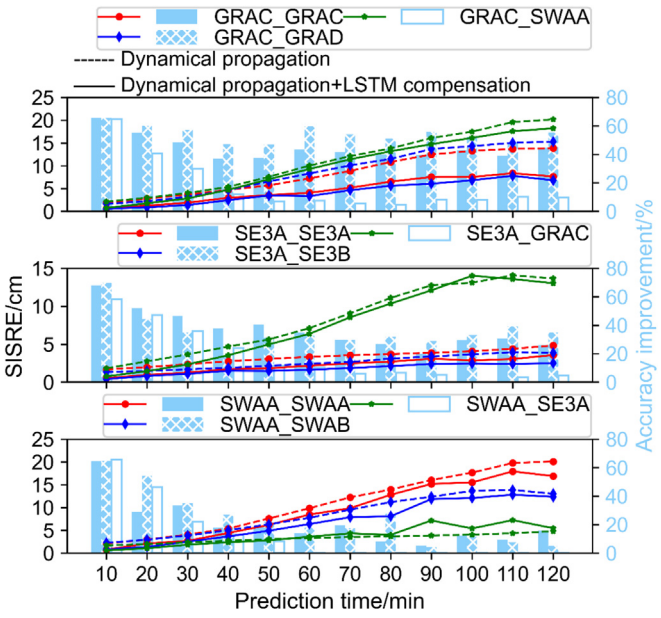

Fig. 11. SISRE of predicted orbits with and without compensation of the LSTM model from the generalization tests between different LEO satellites (Dotted lines refer to results without compensation and solid lines refer to results with compensation; Light blue bars represent the orbit accuracy improvement brought by the LSTM model; Lines with different colors refer to the combination of different LEO satellites).

the orbit accuracy improvement gradually decreases to less than 10 % for the 120 min-prediction for "GRAC_SWAA" solution. This may be associated with the orbital altitude/-plane difference between the two satellites. Datasets from two satellites with similar orbital altitude and orbital plane might present similar characteristics, making the trained model suited for both satellites. Conversely, the orbital altitude/plane difference can result in the dissimilar characteristics of datasets which might lead to the inapplicability of the trained model.

As expected, the performance of the LSTM model exhibits commendable generalization ability in the tests of "SE3A_SE3B" solution. We observe the negative accuracy improvement of predicted orbit brought by the LSTM model for the "SWAA_SE3A" solution when the prediction time exceeds 50 min. The large orbital altitude/plane difference between these two satellites might be the main cause for the negative values of the orbit accuracy improvement. Therefore, our findings demonstrate that the LSTM model, trained using datasets from a single LEO satellite, is more suitable for predicting orbit errors of various LEO satellites with comparable orbital altitude and orbital plane as the prediction time increases.

5. Discussion

We primarily focus on improving LEO short-term orbit prediction using the LSTM model in this study, thus potentially contributing to the implementation of future LEO-augmented navigation applications. As demonstrated by

the aforementioned results, the LSTM model presents a good performance in improving orbit prediction of LEO satellites within 120 min by yielding a significant accuracy improvement of more than 30 % for different LEO satellites. Despite these promising results, the orbit prediction time is confined to 120 min, and one may also be concerned with how the LSTM model performs in orbit prediction of LEO satellites with longer time. Thereby, we will make a discussion about the potential of the LSTM model in improving LEO long-term orbit prediction in this section. Considering the anomalously quiet solar conditions in 2019, we also present the experimental results of short-term orbit prediction of LEO satellite during the period of elevated solar radiation. Finally, we provide the possible physical explanations for why the LSTM model can effectively improve the accuracy of the dynamical-propagation-based predicted orbit.

We design seven solutions that cover a prediction time from one day to seven days to assess the performance of LSTM model in LEO long-term orbit prediction. A typical LEO satellite (GRACE-C) is selected to carry out the experiments. Following the conclusion that a large NF is more suitable for orbit prediction of LEO satellites exceeding 60 min as indicated in Section 4.1, we employ a maximum NF (all filtered features) in the subsequent experiments. Meanwhile, the WL is set to a minimal value (one epoch) to conserve computational resources. In Fig. 12, we show the experimental results with the prediction time from one day to seven days. Different from the results of LEO short-term orbit prediction, the orbit errors can reach meter level when the prediction time is one day based on the dynamical propagation method. As expected, the increase of prediction time brings about a significant enlargement of orbit errors which are roughly several kilometers when the prediction time reaches seven days. Such a rapid divergence of orbit errors provides evidence for the limitation of the dynamical propagation method in orbit prediction of LEO satellites. After the compensation from the LSTM model, the SISRE gains a notable reduction from (17.0, 64.6, 143.6, 254.6, 396.8, 569.3, 772.7) m to (6.7, 22.7, 50.6, 121.1, 146.3, 232.9, 415.9) m with the accuracy improvement of (60.6 %, 64.9 %, 64.8 %, 52.4 %, 63.1 %, 59.1 %, 46.2 %) on average for the solution with prediction time from one day to seven days, respectively. It suggests that our LSTM model can markedly improve the accuracy of orbit prediction of LEO satellites longer than one day, demonstrating its superior performance in improving LEO long-term orbit prediction.

The datasets used for LSTM model training and testing in this study span January to December 2019, corresponding to anomalously quiet solar conditions (F10.7 flux averaging 68 ± 3 sfu). In order to investigate how the LSTM model performs during periods of elevated solar radiation, we implement additional experiments in which the original datasets are extended to cover periods of enhanced solar radiation. A critical case study focuses on 17 April–16 May 2024, a period marked by three G2-class geomagnetic storms (Kp ≥ 6) and eleven M1.0 + solar flares, during which the datasets of short-term orbit prediction from GRACE-C satellite (30 days) were acquired. The training datasets comprise the former 20-day datasets and the original datasets from 2019, while the testing datasets cover the remaining 10 days.

Fig. 13 shows the testing results of orbit prediction of GRACE-C satellite. In comparison with the results from Fig. 9, the orbit prediction results from the dynamical propagation present lower accuracy, which can be explained by the elevated solar activity. This reveals the significant impact of solar activities on orbit prediction of LEO satellites. With the compensation of the LSTM model, the accuracy of short-term orbit prediction gains pronounced improvement. For the prediction time of

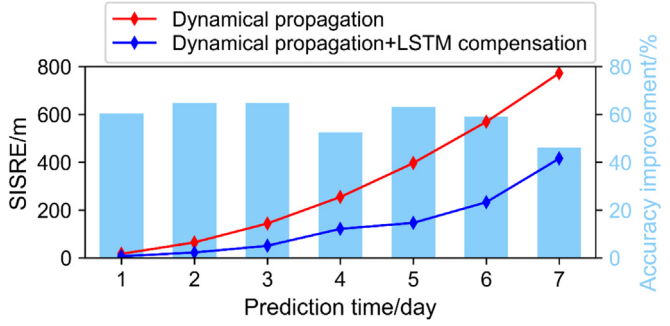

Fig. 12. SISRE of predicted orbits with and without compensation of the LSTM model in three directions of GRACE-C satellite from one day to seven days (Red lines represent results without compensation; Blue lines represent results with compensation; Light blue bars represent the accuracy improvement).

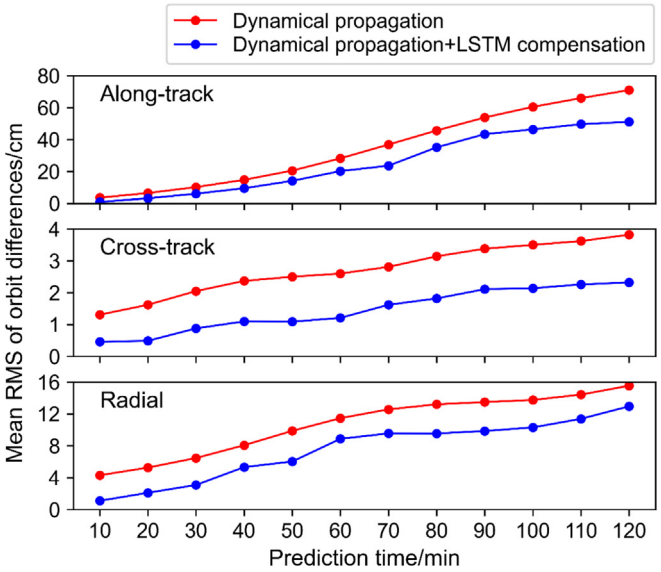

Fig. 13. Mean RMS of orbit differences between PSO products and predicted orbits with and without compensation of the LSTM model in three directions of GRACE-C satellite during the period of elevated solar radiation (Red lines represent results without compensation; Blue lines represent results with compensation).

120 min, the mean RMS of orbit differences get reduced from (71.0, 3.8, 15.5) to (51.1, 2.3, 13.0) cm with the reduction percentage of (28.0 %, 39.5 %, 16.1 %) in three directions, respectively. These findings demonstrate the advantage of the LSTM model in improving the accuracy of orbit prediction of LEO satellites during periods of elevated solar radiation. It suggests that the LSTM model has the great potential of improving LEO short-term orbit prediction even under extreme space weather.

Our findings are encouraging and suggest that the LSTM model can not only improve LEO short-term orbit prediction less than 120 min, but also remarkably reduce the divergence of orbit prediction errors for the prediction longer than one day. Moreover, significant accuracy improvement of orbit prediction of LEO satellites can still be achieved by the LSTM model even during periods of elevated solar radiation. As indicated by the aforementioned results, several features, including "GEO_A", "PC_Su", and "SOL_F", contribute a lot to the orbit prediction errors. These features are strongly linked with the atmosphere drag and solar radiation pressure acting on LEO satellites, which typically represent the primary nonconservative forces for LEO satellites. The imperfections of these nonconservative force models result in the rapid divergence of dynamical-propagation-based orbit prediction errors. Thus, we can reason that the forecasted orbit prediction errors primarily reflect the unmodeled errors of nonconservative forces during the orbit prediction. With the compensation from the LSTM model, the negative impact brought by the mismodeled errors of nonconservative forces can be effectively mitigated, thus contributing to the accuracy improvement. This also provides the explanation for the good generalization ability of the LSTM model among different LEO satellites with comparable orbital altitude and orbital plane, such as GRACE-C and GRACE-D. For these LEO satellites, the nonconservative forces present comparable variations, resulting in the similar characteristics of orbit prediction errors. As such, the orbit prediction accuracy of one LEO satellite can still gain improvement even using the trained model from another LEO satellite. Our results have demonstrated the great potential of machine learning algorithms in orbit prediction of LEO satellites. With the continuously expanded computing power and rapid advancements in machine learning techniques, further improvements in the orbit prediction for large LEO constellations through machine learning methods can be expected, thereby contributing to more high-accuracy applications of LEO satellites.

6. Conclusions

We have investigated improving LEO short-term orbit prediction (less than 120 min) using the LSTM model. Datasets of seven LEO satellites from DOY 001, 2019 to DOY 365, 2019 have been constructed for the experiments. Based on these datasets, the performance of the LSTM model in orbit prediction for different LEO satellites is investigated in detail. Generalization tests between different LEO satellites have also been implemented to validate the generalization ability of the LSTM model.

The impact of NF and WL on the model performance is assessed first. Our results reveal that the model with a small NF and large WL presents superior performance for the extremely short orbit prediction (less than 20 min). In contrast, a large NF is more suitable for orbit prediction of LEO satellites exceeding 60 min. Based on the optimal configuration, the accuracy improvement of 10 min-predicted orbit brought by the LSTM model can reach (59.3 %, 74.8 %, 71.1 %) in three directions for GRACE-C satellite. When the prediction time reaches 120 min, the orbit accuracy improvement can still reach (49.4 %, 34.3 %, 29.9 %). The overall orbit accuracy improvement brought by the LSTM model exceeds 30 % with a maximum value around 75 % and the P value is less than 0.8 with a minimum value around 0.2. With the improvement of the LSTM model, the prediction time for obtaining 5-cm accuracy of predicted orbit can be extended to (41.2, 42.0, 31.2, 37.9, 30.0, 86.3, 108.1) min for GRACE-C/D, Swarm-A/B/C, and Sentinel-3A/3B satellites, respectively. Generalization tests between different LEO satellites reveal that the LSTM model is of commendable generalization ability for the extremely short-term prediction (less than 30 min) across different satellites. As the prediction time increases, the LSTM model trained using datasets from a single LEO satellite is more suitable for forecasting orbit prediction errors of various LEO satellites with comparable orbital altitude and orbital plane.

Our findings have demonstrated the great potential of the LSTM model in improving LEO short-term orbit prediction. Future research may extend the selection of the LSTM model to multiple different machine learning models and investigate the applicability of these models in the orbit prediction for different LEO satellites. With the advancements in machine learning techniques in the future, further improvements in the orbit prediction for large LEO constellations through machine learning methods are foreseeable.

Declaration of competing interest

The authors declare that they have no known competing financial interests or personal relationships that could have appeared to influence the work reported in this paper.

Acknowledgements

This study is financially supported by the National Natural Science Foundation of China (No. 41974027), the National Key Research and Development Program of China (2021YFB2501102), the Hubei Province Natural Science Foundation (Grant No. 2020CFA002) and the Sino-German mobility programme (Grant No. M-0054). Thanks goes to ESA (ftp://swarm-diss.eo.esa.int), CPOD ( ), and JPL (ftp://anonymous@isdcftp.gfz-potsdam.de/

grace-fo/Level-1B/JPL/INSTRUMENT/RL04) for providing precise science orbit products and onboard GNSS observations of LEO satellites. The numerical calculations in this paper have been done on the supercomputing system in the Supercomputing Center of Wuhan University.

Appendix A. Analysis of computational resource consumption

Apart from the accuracy improvement of orbit prediction of LEO satellites brought by the LSTM model, the computational resource consumption is also vital in practical applications. In Table A1, we show the computational resource consumption during the model training and testing for the 120-min orbit prediction of GRACE-C satellite. The sample size is 118,243 (272 orbit arcs) and 29,561 (68 orbit arcs) for model training and model testing, respectively. The total time consumption is 873 s for model training. By comparison, model testing consumes more time that reaches 1069 s. This is because the input window needs to be updated with the former forecasted result each time during model testing. Considering that the testing datasets cover 68 orbit arcs, the time consumption for forecasting the orbit prediction errors of a 120-min orbit arc is roughly 16 s. A smaller time consumption is required if the prediction arc is shorter. It indicates that our LSTM model has a high computational efficiency in orbit prediction of LEO satellites.

Table A1
Computational resource consumption during model training and testing for the 120-min orbit prediction of GRACE-C satellite.

Item	Model training	Model testing
Sample size	118,243	29,561
Storage memory	880 Mb	220 Mb
Running memory	2918 Mb	2316 Mb
Time consumption	873 s	1069 s

References

Calero, E. J., Fernández, J., Peter, H., Féménias, P., 2019. Single-receiver ambiguity resolution for precise orbit determination of the Copernicus Sentinel Satellites at the Copernicus POD service. EGU General Assembly, Vol. 7–12, EGU20199070.

Chen, T., Guestrin, C., 2016. Xgboost: a scalable-tree boosting system. In: Proceedings of the 22nd ACM SIGKDD International Conference on Knowledge Discovery and Data Mining, pp. 785–794. https://doi.org/10.1145/2939672.2939785.

Del Portillo, I., Cameron, B.G., Crawley, E.F., 2019. A technical comparison of three low earth orbit satellite constellation systems to provide global broadband. Acta Astronaut. 159, 123–135. https://doi.org/10.1016/j.actaastro.2019.03.040.

Fernández Martìn, C., 2016. Sentinel-3A properties for GPS POD, GMV-GMESPOD-TN-0027, v1.2.

Ge, H., Li, B., Ge, M., Nie, L., Schuh, H., 2020. Improving Low Earth Orbit (LEO) prediction with accelerometer data. Remote Sens. (Basel) 12 (10), 1599. https://doi.org/10.3390/rs12101599.

Gers, F.A., Schmidhuber, J., Cummins, F., 2000. Learning to forget: continual prediction with LSTM. Neural Comput. https://doi.org/10.1049/cp:19991218.

Gou, J., Rösch, C., Shehaj, E., Chen, K., Kiani Shahvandi, M., Soja, B., Rothacher, M., 2023. Modeling the differences between ultra-rapid and final orbit products of GPS satellites using machine-learning approaches. Remote Sens. (Basel) 15, 5585. https://doi.org/10.3390/rs15235585.

He, L., Wang, W., Wu, Z., 2017. Orbit analysis for Tiangong-2 space lab under different perturbation forces. In: Sun, J., Liu, J., Yang, Y., Fan, S., Yu, W. (Eds.), Proceedings of China Satellite Navigation Conference (CSNC) 2017, 23–25 May, Shanghai, China. Springer, Singapore, pp 485–494. doi: 10.1007/978-981-10-4588-2_42.

Hochreiter, S., Schmidhuber, J., 1997. Long short-term memory. Neural Comput. 9 (8), 1735–1780. https://doi.org/10.1162/neco.1997.9.8.1735.

Jäggi, A., Bock, H., Floberghagen, R., 2011. GOCE orbit predictions for SLR tracking. GPS Solut. 15 (2), 129–137.

Jamil, H.A., Nadim, K., Zaher, M.K., 2022. A hybrid analytical-machine learning approach for LEO satellite orbit prediction. 2022 25th International Conference on Information Fusion.

Kazmierski, K., Sośnica, K., Hadas, T., 2018. Quality assessment of multi-GNSS orbits and clocks for real-time precise point positioning. GPS Solut. 22, 11. https://doi.org/10.1007/s10291-017-0678-6.

Li, B., Huang, J., Feng, Y., Wang, F., Sang, J., 2020. A machine learning-based approach for improved orbit predictions of LEO space debris with sparse tracking data from a single station. IEEE Trans. Aerosp. Electron. Syst. 99, 1. https://doi.org/10.1109/TAES.2020.2989067.

Li, X., Ma, F., Li, X., Lv, H., Bian, L., Jiang, Z., Zhang, X., 2019. LEO constellation-augmented multi-GNSS for rapid PPP convergence. J. Geod. 93 (5), 749–764. https://doi.org/10.1007/s00190-018-1195-2.

Liu, L., Wang, Y., 2006. An analytical method for satellite orbit prediction. Chin. Astron. Astrophy 30 (1), 68–74. https://doi.org/10.1016/j.chinastron.2006.01.006.

Lou, Y., Dai, X., Gong, X., Li, C., Qing, Y., Liu, Y., Peng, Y., Gu, S., 2022. A review of real-time multi-GNSS precise orbit determination based on the filter method. Satell. Navig. 3, 15. https://doi.org/10.1186/s43020-022-00075-1.

Montenbruck, O., Hackel, S., van den Ijssel, J., Arnold, D., 2018. Reduced dynamic and kinematic precise orbit determination for the Swarm mission from 4 years of GPS tracking. GPS Solut. 22, 79. https://doi.org/10.1007/s10291-018-0746-6.

Nair, V., Hinton, G.E., 2010. Rectified linear units improve restricted Boltzmann machines. In: Proceedings of the 27th International Conference on Machine Learning (ICML-10), Haifa, Israel, June, pp. 807–814.

Olsen, N., Friis-Christensen, E., Floberhagen, R., Alken, P., Beggan, C., Chulliat, A., Doornbos, E., Teixeira da Encarnação, J., Hamilton, B., Hulot, G., van den IJssel, J., Kuvshinov, A., Lesur, V., Lühr, H., Macmillan, S., Maus, S., Noja, M., Olsen, P., Park, J., Plank, G., Püthe, Ch., Rauberg, J., Ritter, P., Rother, M., Sabaka, T., Schachtschneider, R., Sirol, O., Stolle, C., Thébault, E., Thomson, A., Tøffner-Clausen, L., Velímský, J., Vigneron, P., Visser, P., 2013. The swarm satellite constellation application and research facility (SCARF) and swarm data products. Earth Planets Space 65 (11), 1189–1200. https://doi.org/10.5047/eps.2013.07.001.

Peng, H., Bai, X., 2018. Improving orbit prediction accuracy through supervised machine learning. Adv. Space Res. 61 (10), 2628–2646. https://doi.org/10.1016/j.asr.2018.03.001.

Peng, H., Bai, X., 2019. Comparative evaluation of three machine learning algorithms on improving orbit prediction accuracy. Astrodynamics 3 (4), 325–343. https://doi.org/10.1007/s42064-018-0055-4.

Petit, G., Luzum, B., 2010. IERS Conventions (2010). IERS Technical Note 36.

Picone, J.M., Hedin, A.E., Drob, D.P., Aikin, A.C., 2002. NRLMSISE-00 empirical model of the atmosphere: statistical comparisons and scientific issues. J. Geophys. Res. 107 (A12), SIA 15-1–SIA 15-16. https://doi.org/10.1029/2002JA009430.

Pintas, J.T., Fernandes, L.A.F., Garcia, A.C.B., 2021. Feature selection methods for text classification: a systematic literature review. Artif. Intell. Rev. 54, 6149–6200. https://doi.org/10.1007/s10462-021-09970-6.

Reid, T.G.R., Neish, A.M., Walter, T.F., Enge, P.K., 2016. Leveraging commercial broadband LEO constellations for navigation. In: Proceedings of the 29th International Technical Meeting of the Satellite Division of The Institute of Navigation (ION GNSS+ 2016), Portland, Oregon, September, 2300–2314. doi: 10.33012/2016.14729.

Salleh, N.A., Yuhaniz, S., Azmi, N.F.M., Sabri, S.F., 2019. Enhancing simplified general perturbations-4 model for orbit propagation using deep learning: a review. In: Proceedings of the 2019 8th International Conference on Software and Computer Applications, pp. 27–32. https://doi.org/10.1145/3316615.3316675.

Shao, K., Gu, D., Ju, B., Wang, W., Wei, C., Duan, X., Wang, Z., 2020. Analysis of Tiangong-2 orbit determination and prediction using onboard dual-frequency GNSS data. GPS Solut. 24 (1), 11. https://doi.org/10.1007/s10291-019-0927-y.

Şimşek, M., Taşkıran, M., Doğan, U., 2025. Modelling of GNSS station position time series using deep learning approaches. Earth Sci. Inform. 18, 96. https://doi.org/10.1007/s12145-024-01576-0.

Wen, H., Kruizinga, G., Paik, M., Landerer, F., Bertiger, W., Sakumura, C., Bandikova, T., Mccullough, C., 2019. Gravity Recovery and Climate Experiment Follow-on (GRACE-FO) level-1 data product user handbook. p. 56935.

Xie, X., Geng, T., Zhao, Q., Liu, X., Zhang, Q., Liu, J., 2018. Design and validation of broadcast ephemeris for low Earth orbit satellites. GPS Solut. 22, 54. https://doi.org/10.1007/s10291-018-0719-9.

Yu, Y., Si, X.S., Hu, C.H., Zhang, J.X., 2019. A review of recurrent neural networks: LSTM cells and network architectures. Neural Comput. 31 (7), 1235–1270. https://doi.org/10.1162/neco_a_01199.

Zhang, K., Li, X., Wu, J., Yuan, Y., Li, X., Zhang, X., Zhang, W., 2021. Precise orbit determination for LEO satellites with ambiguity resolution: improvement and comparison. J. Geophys. Res. Solid Earth 126, e2021JB022491. https://doi.org/10.1029/2021JB022491.